Diurnal Variation of Surface Wind Divergence in the Maritime Continent Using ASCAT and SeaWinds Observations and ERA5 Reanalysis Data

Inovasita Alifdini[1, 2] and Teruhisa Shimada[1]

[1]*Graduate School of Science and Technology, Hirosaki University, Hirosaki, Japan*
[2]*Institute of Meteorology and Climate Research, Department Troposphere Research, Karlsruhe Institute of Technology, Karlsruhe, Germany*

Abstract

This study investigates the diurnal variation of surface wind divergence in the seas of the Maritime Continent by using satellite scatterometer observations and atmospheric reanalysis data. This is the first study to demonstrate the distribution and seasonal variation of the diurnally varying surface winds in the Maritime Continent in terms of wind divergence. Wind divergence develops from the coasts of the islands toward the center of the seas and dominates during the afternoon and evening hours. Wind convergence dominates over the seas during the nighttime and morning hours. The offshore extensions of the wind divergence and convergence from the coast differ regionally and thus show the asymmetric patterns with respect to the center of the seas. In particular, strong wind divergence develops from the southern coasts of the Java Sea and the Arafura Sea to extend northward beyond the center of the seas. The diurnal amplitudes of wind divergence vary seasonally and reach a peak in September in most of the seas. The switching times between wind divergence and convergence are almost fixed throughout the year regardless of the monsoon reversal.

(**Citation**: Alifdini, I., and T. Shimada, 2022: Diurnal variation of surface wind divergence in the Maritime Continent using ASCAT and SeaWinds observations and ERA5 reanalysis data. *SOLA*, **18**, 154−158, doi:10.2151/sola.2022-025.)

1. Introduction

Wind divergence exerts a crucial influence on the climate of the Maritime Continent (MC). Strong wind convergence arising from diurnal variation in wind induces diurnal variation in heavy rainfall over the mountains in Sumatra and Java islands (Arakawa and Kitoh 2005; Qian et al. 2010). The low-level wind convergence induced by valley winds initiates convection over western Java Island (Oigawa et al. 2017). The topography of the islands modulates moisture convergence induced by surface winds and the resulting convection (Wu and Hsu 2009). The strong wind divergence along the mountain contributes to the offshore propagation of rainfall from the coasts of western Sumatra and northern Java Islands (Im and Eltahir 2018). Large-scale divergent winds reduce the middepth transport of the Indonesian throughflow (Potemra and Schneider 2007). Thus, the wind divergence is a key factor for various atmospheric and oceanic processes in the MC with complex topography and land-sea contrast.

However, the analyses of the diurnally varying winds and the resulting wind divergence are limited to the target region. We have not yet fully understood the systematic diurnal variations and organized distributions of wind divergence in the MC. In addition, we need to investigate seasonal variations in the diurnal amplitudes of wind divergence. The following two studies focus on the diurnal variation of surface winds over the MC as a whole. Short et al. (2019) have defined a wind perturbation relative to the background wind to explore the diurnal variation in surface winds between the observation times of the scatterometers. Alifdini et al. (2021) have demonstrated that the diurnally varying components of surface wind have a maximum magnitude in September along the northern coasts of Java Island and the small islands to the east, along the northwest and northeast coasts of Borneo, along the coast of southern Sulawesi Island, and to the southwest of Papua Island. In response to these two investigations, we need to examine the diurnal variation in wind divergence to elucidate the diurnally varying processes in the MC.

The present study explores the diurnal variation in surface wind divergence by analyzing wind data from satellite scatterometer observations and atmospheric reanalysis. Wind divergence enables effective analysis of diurnally varying wind because land-sea breeze is associated with surface wind divergence and convergence (Dai and Desser 1999). Alifdini et al. (2021) have shown that the diurnal variation of surface winds is prominent in September, when the Australian winter monsoon dominates over the MC (Fig. 1). Therefore, we mainly focus on the diurnal variation in surface wind divergence in September and then show the seasonal variation in diurnal amplitudes of wind divergence.

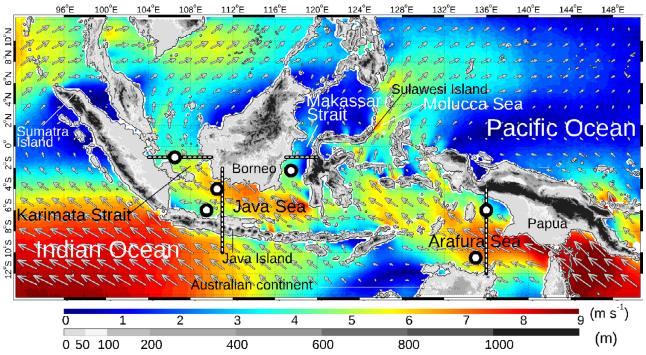

Fig. 1. Monthly means of wind vectors in September derived from ASCAT (2010−2018) with geographical names. We plotted the vectors at every 12 grid points (1.5° × 1.5°). The color shading shows wind speeds. The gray-scale shading represents the topographic elevation. Four black solid lines overlapped with white dashed lines denote the sections for the analyses in Fig. 4. Six black-white circles indicate the selected locations for the analyses in Fig. 5.

2. Data and method

We used scatterometer wind measurements at 10 m with a grid size of 12.5 km acquired by the Advanced SCATterometer (ASCAT) onboard Meteorological Operational-A (MetOp-A) and Meteorological Operational-B (MetOp-B) satellites (2010−2018) (EUMETSAT/OSI SAF 2010, 2013) and by SeaWinds onboard QuikSCAT (1999−2009) (SeaPAC 2018). The MetOp-A and MetOp-B satellites cross the equator in the MC at 09:30 LT on the descending node and at 21:30 LT on the ascending node. The equatorial crossing times of QuikSCAT are at approximately 06:00 LT on the ascending node and 18:00 LT on the descending node (Gille et al. 2003). The combined use of the ASCAT and SeaWinds

Corresponding author: Inovasita Alifdini, Institute of Meteorology and Climate Research, Department Troposphere Research, Karlsruhe Institute of Technology, Karlsruhe, Germany. E-mail: inovasita.alifdini@kit.edu.

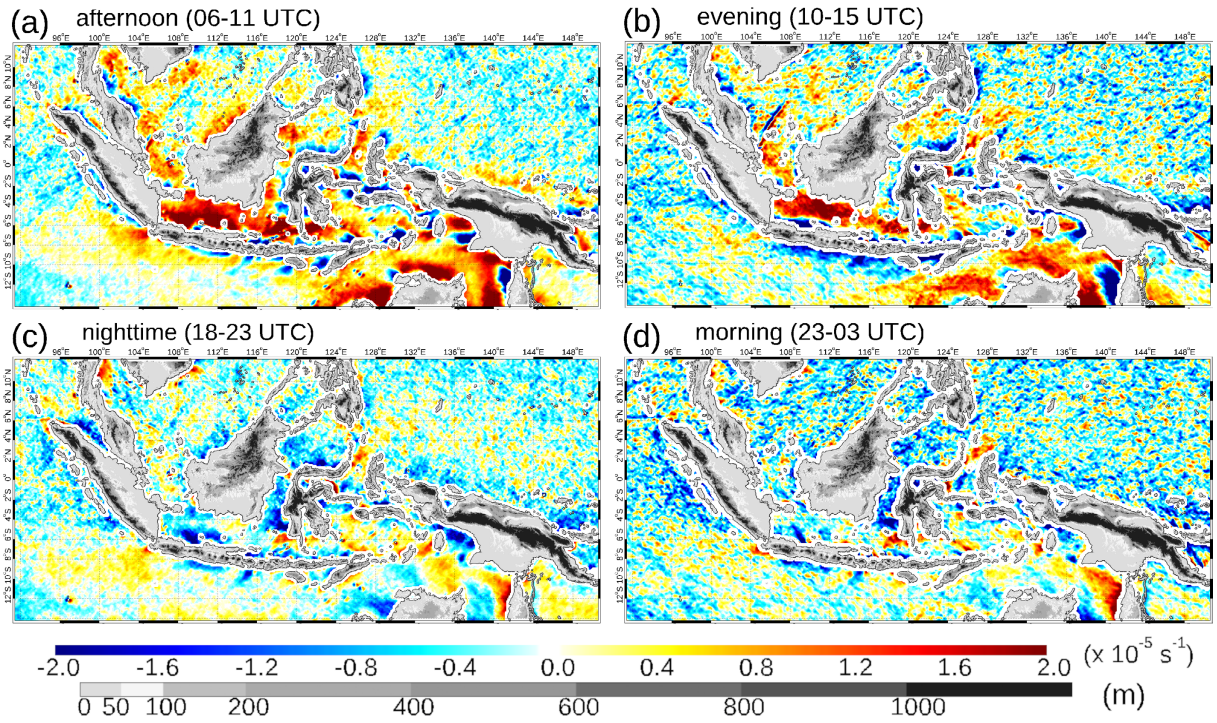

Fig. 2. Means of wind divergence in September from (a, c) QuikSCAT and (b, d) ASCAT during the (a) afternoon (06−11 UTC), (b) evening (10−15 UTC), (c) nighttime (18−23 UTC), and (d) morning (23−03 UTC) hours.

data allows us to provide observational evidence of diurnal variation in surface wind divergence, which has not been analyzed in the climatological studies using scatterometers (Chelton et al. 2004; Luis and Pandey 2005; and Wood et al. 2009). In addition, we used hourly winds at a 10 m height from the fifth-generation European Centre for Medium-Range Weather Forecasts atmospheric reanalysis (ERA5) (2010−2018) with a grid size of 0.25° (Hersbach et al. 2018; 2020). The hourly data from ERA5 allow us to adequately analyze diurnally varying winds. The spatial grid size of 0.25° enables the analysis of winds in the MC. We computed wind divergence at each grid cell using the two-dimensional Gauss' divergence theorem: $\nabla \cdot \boldsymbol{u} \approx \frac{1}{S}\oint_C \boldsymbol{u}\cdot\boldsymbol{n}dl$ where $\boldsymbol{u}$ is the horizontal wind vector, S is the integration area of a given grid cell, and $\boldsymbol{n}$ is the unit vector with rightward direction along the line element (dl) of the integration path (C).

3. Results

3.1 Regional distributions

We examine the diurnal variation in wind divergence from the climatology in September derived from the scatterometer data (ASCAT and SeaWinds) on the basis of the passing times of the satellites (Fig. 2). The most prominent feature is that diurnally varying winds switch between divergence and convergence of the surface wind in the MC. Wind divergence dominates during the afternoon and evening hours (Figs. 2a and 2b). The maximum magnitudes ($> 2.0 \times 10^{-5}$ s^{-1}) are found near the coast in the afternoon (Fig. 2a). Wind convergence dominates during the nighttime and morning hours (Figs. 2c and 2d). The magnitude of wind divergence becomes smaller during the nighttime and morning hours than during the afternoon and evening hours, even where the wind divergence persists. These results mean that sea surface winds in the seas of the MC diverge due to sea breeze and converge due to land breeze owing to the land-sea contrast and that the land-sea breeze circulations extend across the seas.

The diurnal variations in wind divergence described above are consistent with those derived from the ERA5 data (Fig. 3). The overall distributions of the wind divergence bear a close resemblance between the scatterometer data and the ERA5 data. The differences in the wind divergence between the two datasets are as follows. First, the distributions derived from the scatterometer data are slightly noisy owing to the limited data. Second, the magnitudes of divergence and convergence are underestimated and the distributions are smoothed for the ERA5 data owing to the grid size of 0.25°. Then, the ERA5 data enhances the divergence and convergence near the coast, especially in the Java Sea and around Borneo during the afternoon hours. However, the wind divergence fields derived from the scatterometer data and the ERA5 data show no significant differences in the distributions. This is supported by the fact that Alifdini et al. (2021) derived the consistent results from the scatterometer and ERA5 datasets. Although the ERA5 wind data have systematic errors in the wind components and the resulting weak convergence generally in the tropics (Rivas et al. 2019), a comparison of the wind divergence derived from the two datasets in the MC shows linear relationships with negligible biases enough to explore the diurnal distribution of wind divergence (Supplement 1). Therefore, we can conclude that the consistency of the diurnal variations between the two datasets allows us to explore the features region by region.

We examine regional distribution and diurnal variation of the wind divergence from the common features derived from the scatterometer data and the ERA5 data (Figs. 2 and 3). The Java Sea and Arafura Sea exhibit distinct features. The strong wind divergence ($> 2.0 \times 10^{-5}$ s^{-1}) develops from the northern seaboards of Java Island and the Australian continent during the afternoon hours and extends northward over the entire seas during the evening hours (Figs. 2a and 2b; Figs. 3a and 3b). The most significant diurnal variation in wind divergence occurs over the Java Sea, which is consistent with the analysis along the transect by Short et al. (2019). The exceptional feature is that wind convergence develops during the afternoon and evening hours (Figs. 2a and 2b; Figs. 3a and 3b), and divergence persists during the nighttime and morning hours (Figs. 2c and 2d; Figs. 3c and 3d) in the gulf off Australia (11°S/141°E). Strong convergence similarly develops off the southwest coast of Papua Island (7°S/137°E) during the afternoon and evening hours (Figs. 2a and 2b; Figs. 3a and 3b). In

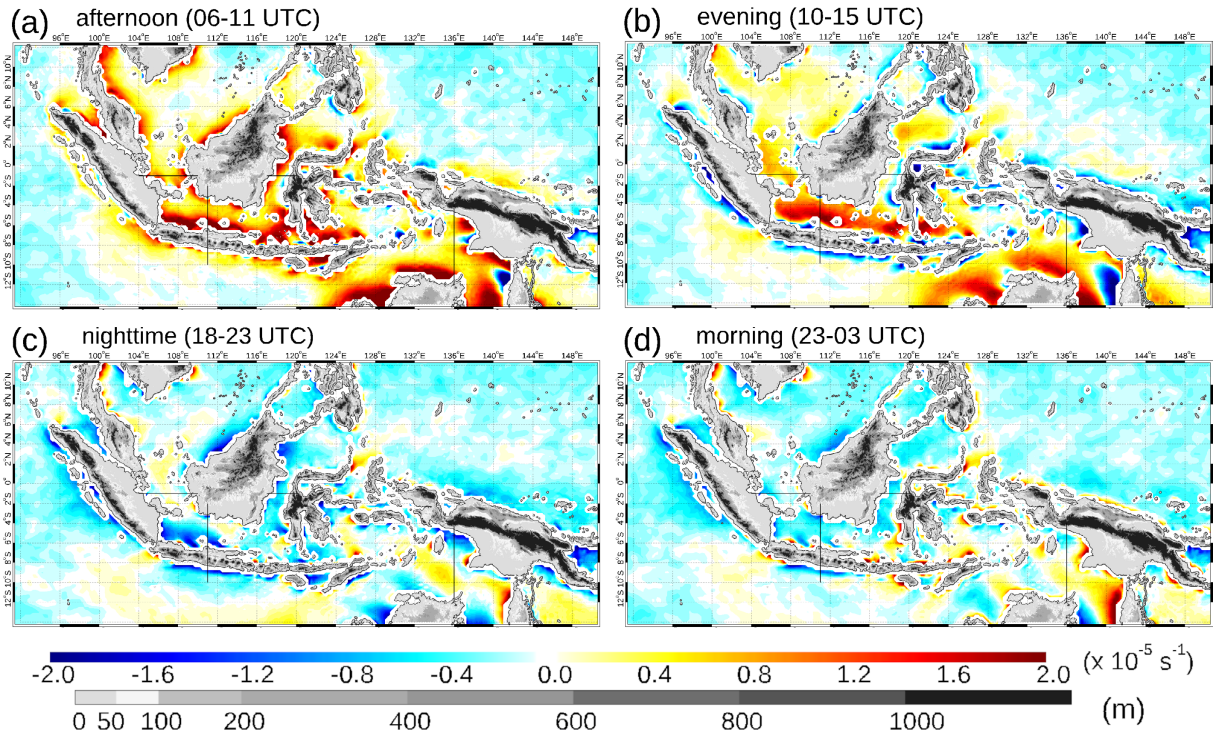

Fig. 3. Means of wind divergence in September from ERA5 (2010−2018) during the (a) afternoon (06−11 UTC), (b) evening (10−15 UTC), (c) nighttime (18−23 UTC), and (d) morning (23−03 UTC) hours. The color range is the same as in Fig. 2. Four black solid lines in each panel denote the sections for the analyses in Fig. 4.

the northern Molucca Sea (2°N/126°E), wind divergence persists throughout the day (Figs. 2 and 3) owing to the strong winds outflowing from the Molucca Sea to the Pacific Ocean (Fig. 1). In the open oceans surrounding the MC, convergence persists throughout the day with little diurnal variation.

3.2 Offshore propagation

To examine how the diurnal variation in wind divergence extends over the seas and propagates offshore, we made Hovmöller diagrams of wind divergence along the selected sections (Fig. 4). These sections are located on the monsoon routes. The Hovmöller diagrams commonly show that wind divergence starts to develop at approximately 10 LT to extend offshore and lasts until approximately 20 LT, as described above. However, the speeds of the offshore extension of divergence from the coast differ from region to region and thus the diagrams show the asymmetric patterns with respect to the center of the seas.

Strong wind divergence develops from the coast in the east and west of the Karimata Strait and propagates to the center of the strait between 10 LT and 20 LT (Fig. 4a). Although the peak of wind divergence ($> 2.0 \times 10^{-5}$ s^{-1}) in the western seaboard of Borneo Island (109.0°E) occurs two hours earlier than in the eastern seaboard of Sumatra Island (104.8°E), the divergence propagates toward the center of the strait more slowly in the east of the strait than in the west. On the other hand, strong wind convergence ($< -1.2 \times 10^{-5}$ s^{-1}) occurs in the eastern seaboard of Sumatra Island between 4 LT and 9 LT and propagates to the center of the strait up to 107.5°E. In the western seaboard of Borneo Island, weak convergence propagates westward over the same distance from the coast as divergence does.

The switch between wind divergence and convergence is clearly visible in the Makassar Strait (Fig. 4b). Stronger divergence develops in the eastern seaboard of Borneo Island than in the western seaboard of Sulawesi Island. The duration of the divergence decreases with increasing distance from the coast of Borneo Island, and convergence dominates during the evening and nighttime hours in the east.

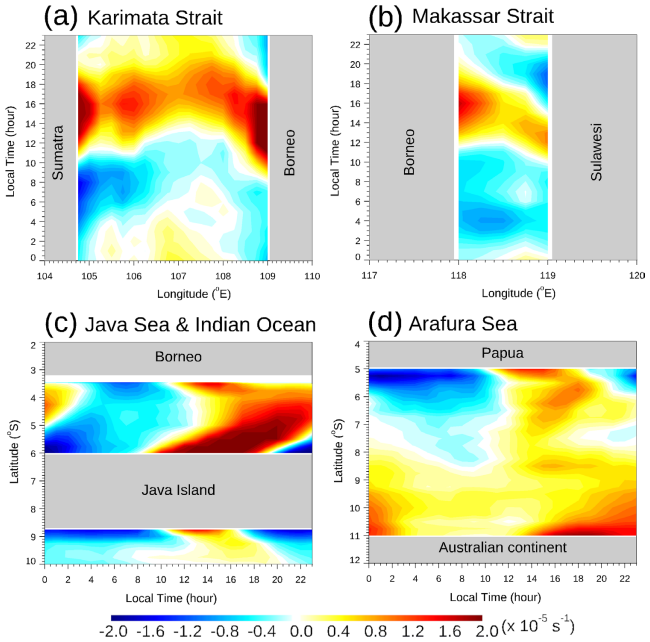

Fig. 4. Diurnal Hovmöller diagrams of wind divergence in September derived from ERA5 (2010−2018) along the selected sections shown in Figs. 1 and 3. (a) Karimata Strait (1°S), (b) Makassar Strait (1°S), (c) Java Sea and Indian Ocean (111°E), and (d) Arafura Sea (136°E). Note that the axes are switched between (a, b) and (c, d). We extracted the data along the sections at every 0.25° interval. The light gray color denotes the land. The local times are UTC + 07:00 in (a, c), UTC + 08:00 in (b), and UTC + 09:00 in (d).

Wind divergence and convergence clearly switch in the Java Sea (Fig. 4c). The strong wind divergence develops from the northern seaboard of Java Island (6°S) two hours earlier than from the southern seaboard of Borneo Island (3.3°S). Moreover, the divergence extending from the south and north merges at around 4°S and the propagation distance from the south reaches two-thirds of the north-south distance of the Java Sea. Wind convergence developing from the northern seaboard of Java Island also propagates further into the Java Sea than that from the southern seaboard of Borneo Island. In contrast, in the southern seaboard of Java Island (8.8°S–10.0°S), the maximum magnitudes of wind divergence and convergence are smaller than those in the Java Sea, and are confined to the vicinity of the southern coast of Java Island.

In the northern Arafura Sea or to the south of Papua Island (5°S–8°S), wind divergence during the daytime hours and convergence during the nighttime hours switches (Fig. 4d). In contrast, the wind divergence dominates and persists throughout the day in the southern Arafura Sea (8°S–11°S). The strong divergence ($> 2.0 \times 10^{-5}$ s^{-1}) appears near the northern coast of the Australian continent (11°S) during 14–20 LT and propagates to the north.

3.3 Seasonal variation

Finally, we show how the diurnal variation in wind divergence changes seasonally at the selected locations (Fig. 5). The results generally share the following three key characteristics. First, the amplitude of the wind divergence changes seasonally, whereas the switching times between wind divergence and convergence are almost fixed throughout the year (Supplement 2). In other words, the diurnal phases of wind divergence are nearly independent of the monsoon reversal (e.g., Figs. 2 and 3 of Alifdini et al. 2021). Second, the seasonal variations in wind divergence during the daytime hours are larger than those in wind convergence during the nighttime hours. In particular, the magnitudes of the convergence during the nighttime hours vary little throughout the year in the following four regions: the Karimata Strait, the Makassar Strait, the northern Java Sea, and the southern Arafura Sea (Figs. 5a, 5b, 5c, and 5f). These results mean that the seasonally varying magnitudes of wind divergence during the daytime hours mainly create the seasonal variations in wind divergence. Moreover, the magnitudes of wind divergence are generally larger in May–October or during the Australian winter monsoon than in December–March or during the East Asian winter monsoon, except in the Makassar Strait (Figs. 5a, 5c, 5d, 5e, and 5f).

In the Karimata Strait, the wind divergence shows a peak in September with a magnitude of 1.0×10^{-5} s^{-1} at 16 LT (Fig. 5a). The seasonal variation in the Makassar Strait is similar to that in the Karimata Strait, whereas the magnitude of wind divergence reaches a peak (1.75×10^{-5} s^{-1}) in January–March (Fig. 5b). In the northern Java Sea, wind divergence and convergence develop diurnally throughout the year (Fig. 5c). In May–October, the duration of wind divergence is long (12–3 LT). In the northern Arafura Sea, diurnal variations differ according to the monsoons (Fig. 5d). When the Australian winter monsoon dominates in May–October, wind divergence and convergence develop and reach a peak in September. When the East Asian winter monsoon dominates in December–March, the divergence weakly develops and the convergence shows little growth. In the southern Java Sea, both wind divergence during the daytime hours and wind convergence during the nighttime hours exhibit significant seasonal variation and the seasonal amplitudes are the largest in the MC (Fig. 5e). The wind divergence reaches 3.5×10^{-5} s^{-1} in September and decreases to 0.9×10^{-5} s^{-1} in January. The wind convergence reaches -2.2×10^{-5} s^{-1} in August. In the southern Arafura Sea, diurnal variations differ according to the monsoons (Fig. 5f), which is consistent with those in the northern Arafura Sea (Fig. 5d). The wind divergence significantly develops and lasts for a day in May–October or during the Australian winter monsoon (Fig. 5f). This difference between the monsoon seasons indicates that the spatial extent and magnitude of diurnally varying winds near the northern coast of the Australian continent, which are analyzed during the East Asian winter monsoon by Brown et al. (2017), are significantly enhanced during the Australian winter monsoon.

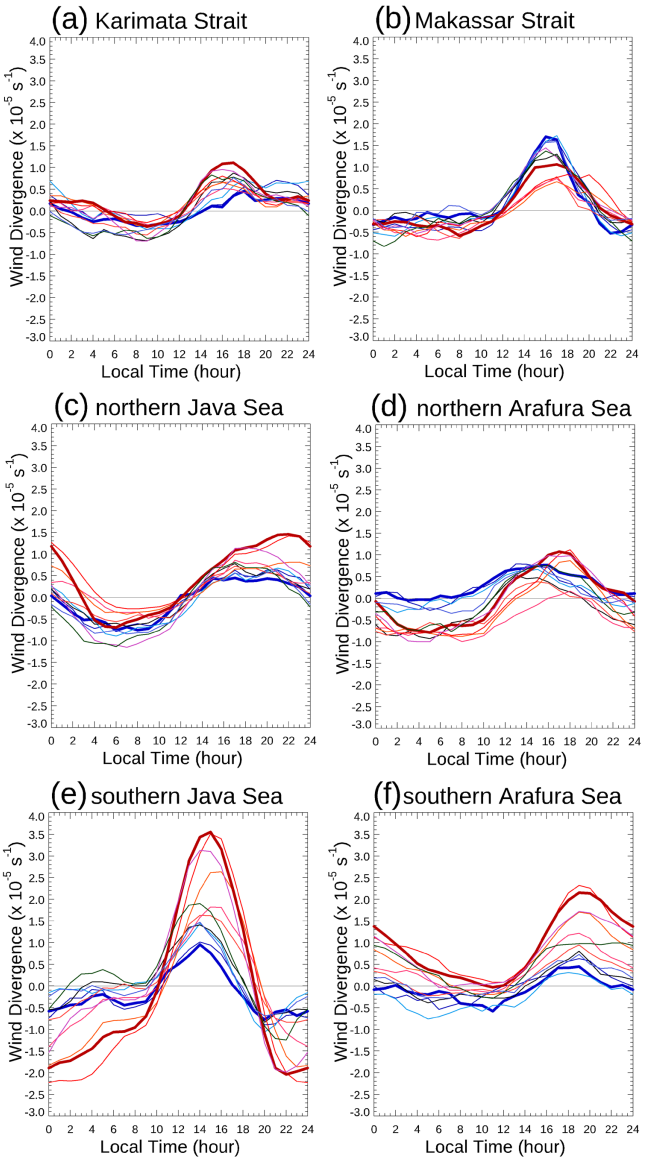

Fig. 5. Monthly changes in diurnal variations of wind divergence derived from ERA5 (2010–2018) at the selected six locations denoted by black-white points in Fig. 1. (a) Karimata Strait (106.5°E, 1.0°S), (b) Makassar Strait (117.5°E, 2.25°S), (c) northern Java Sea (109.5°E, 6.0°S), (d) northern Arafura Sea 136.0°E, 6.0°S), (e) southern Java Sea (109.5°E, 6.0°S), and (f) southern Arafura Sea (135.0°E, 10.5°S). The months of the data are shown in different colors at the bottom of the figure. Cool colors are used for the typical months of the East Asian winter monsoon (December–March), and warm colors are used for the typical months of the Australian winter monsoon (May–October). The bold blue and red lines represent the wind divergence in January and September, respectively.

4. Summary and discussion

We have presented the diurnal variability in surface wind divergence over the seas in the MC. The main conclusions are summarized below. 1) Wind divergence develops from the coasts of the islands to propagate to the center of the seas during the afternoon to evening hours. Wind convergence covers most of the seas during the morning and nighttime hours. 2) Wind divergence and convergence extend from the coast farther to the inland seas than to the open ocean. The offshore extension of the divergence and convergence differ between the coasts on both sides of the

seas. Significant diurnal variation occurs in the southern Java Sea and the Arafura Sea. 3) The diurnal amplitude of wind divergence changes seasonally, whereas the switching times between the wind divergence and convergence are almost fixed throughout the year. In contrast, the seasonally varying magnitudes of wind divergence during the daytime hours create seasonal variations in wind divergence. The magnitudes of the wind convergence during the nighttime hours vary insignificantly throughout the year. These results demonstrate the validity of wind divergence as a measure of diurnally varying winds distinguished from the prevailing monsoon winds.

Further studies are required to clarify the following points. First, we need to investigate the causes of the regional differences in the diurnal amplitudes of the wind divergence. In particular, the important challenge is to examine the asymmetric offshore propagation of wind divergence and convergence across the seas. We need to clarify the contributions of the following factors: increases in air temperature on the islands and in regional sea surface temperature, the resulting land-sea thermal gradient, topography and sizes of the islands, and the background divergence associated with the monsoon winds. Alifdini et al. (2021) showed that the surface temperature gradients between land and sea are mainly induced by the increase in surface temperature during the daytime. This fact is likely associated with the dominant seasonal variations in wind divergence during the daytime hours. In addition, we hypothesize that the persistent strong divergence near the northern coast of the Australian continent is induced by background divergence and by large diurnal heating of the Australian continent. Second, the relations between the diurnal variability in wind divergence and rainfall merit further research. Diurnal variations in rainfall dominate in the MC (Love et al. 2011; Bergemann et al. 2015; Worku et al. 2019). High rainfall generally occurs over the seas during the nighttime hours, which suggests the importance of wind convergence dominant in most of the seas during the nighttime and morning hours. To address these issues, we need to analyze the three-dimensional atmospheric structures over the islands and the seas with a focus on horizontal wind divergence and vertical motion.

Acknowledgements

This work was supported by JST SICORP Grant Number JPMJSC21E7, Japan. The first author wishes to thank the INPEX Scholarship Foundation, Japan, for supporting this study.

Edited by: T.-Y. Koh

Supplements

Supplement 1: Comparison of the wind divergence derived from the scatterometer data (ASCAT and QuikSCAT) and the ERA5 data (Fig. S1).

Supplement 2: The results in January corresponding to Figs. 3 and 4 (Figs. S2 and S3).

References

Alifdini, I., T. Shimada, and A. Wirasatriya, 2021: Seasonal distribution and variability of surface winds in the Indonesian seas using scatterometer and reanalysis data. *Int. J. Climatol.*, **41**, 4825−4843, doi:10.1002/joc.7101.

Arakawa, O., and A. Kitoh, 2005: Rainfall diurnal variation over the Indonesian Maritime Continent simulated by 20 km-mesh GCM. *SOLA*, **1**, 109−112, doi:10.2151/sola.2005-029.

Bergemann, M., C. Jakob, and T. P. Lane, 2015: Global detection and analysis of coastline-associated rainfall using an objective pattern recognition technique. *J. Climate*, **28**, 7225−7236, doi:10.1175/JCLI-D-15-0098.1.

Brown, A. L., C. L. Vincent, T. P. Lane, E. Short, and H. Nguyen, 2017: Scatterometer estimates of the tropical sea-breeze circulation near Darwin, with comparison to regional models. *Quart. J. Roy. Meteor. Soc.*, **143**, 2818−2831, doi:10.1002/qj.3131.

Chelton, D. B., M. G. Schlax, M. H. Freilich, and R. F. Milliff, 2004: Satellite measurements reveal persistent small-scale features in ocean winds. *Science*, **303**, 978−983, doi:10.1126/science.1091901.

Dai, A., and C. Deser, 1999: Diurnal and semidiurnal variations in global surface wind and divergence fields. *J. Geophys. Res. Atmos.*, **104**, 31109−31125, doi:10.1029/1999JD900927.

EUMETSAT/OSI SAF, 2010: MetOp-A ASCAT Level 2 Ocean Surface Wind Vectors Optimized for Coastal Ocean. Ver. Operational/Near-Real-Time. PO.DAAC, CA, USA (Available online at: https://podaac.jpl.nasa.gov/dataset/ASCATA-L2-Coastal, accessed 9 May 2022).

EUMETSAT/OSI SAF, 2013: MetOp-B ASCAT Level 2 Ocean Surface Wind Vectors Optimized for Coastal Ocean. Ver. Operational/Near-Real-Time. PO.DAAC, CA, USA (Available online at: https://podaac.jpl.nasa.gov/dataset/ASCATB-L2-Coastal, accessed 9 May 2022).

Gille, S. T., S. G. L. Smith, and S. M. Lee, 2003: Measuring the sea breeze from QuikSCAT Scatterometry. *Geophys. Res. Lett.*, **30**, doi:10.1029/2002GL016230.

Hersbach, H., B. Bell, P. Berrisford, G. Biavati, A. Horányi, J. Muñoz Sabater, J. Nicolas, C. Peubey, R. Radu, I. Rozum, D. Schepers, A. Simmons, C. Soci, D. Dee, and J.-N. Thépaut, 2018: ERA5 hourly data on single levels from 1979 to present. *Copernicus Climate Change Service (C3S) Climate Data Store (CDS)*. doi:10.24381/cds.adbb2d47.

Hersbach, H., B. Bell, P. Berrisford, S. Hirahara, A. Horányi, J. Muñoz-Sabater, J. Nicolas, C. Peubey, R. Radu, D. Schepers, A. Simmons, C. Soci, S. Abdalla, X. Abellan, G. Balsamo, P. Bechtold, G. Biavati, J. Bidlot, M. Bonavita, G. D. Chiara, P. Dahlgren, D. Dee, M. Diamantakis, R. Dragani, J. Flemming, R. Forbes, M. Fuentes, A. Geer, L. Haimberger, S. Healy, R. J. Hogan, E. Hólm, M. Janisková, S. Keeley, P. Laloyaux, P. Lopez, C. Lupu, G. Radnoti, P. D. Rosnay, I. Rozum, F. Vamborg, S. Villaume, and J.-N. Thépaut, 2020: The ERA5 global reanalysis. *Quart. J. Roy. Meteor. Soc.*, **146**, 1999−2049, doi:10.1002/qj.3803.

Im, E., and E. A. B. Eltahir, 2018: Simulation of the diurnal variation of rainfall over the western Maritime Continent using a regional climate model. *Climate Dyn.*, **51**, 73−88, doi:10.1007/s00382-017-3907-3.

Love, B. S., A. J. Matthews, and G. M. S. Lister, 2011: The diurnal cycle of precipitation over the Maritime Continent in a high-resolution atmospheric model. *Quart. J. Roy. Meteor. Soc.*, **137**, 934−947, doi:10.1002/qj.809.

Luis, A. J., and P. C. Pandey, 2005: Characteristics of atmospheric divergence and convergence in the Indian Ocean inferred from scatterometer winds. *Remote Sens. Environ.*, **97**, 231−237, doi:10.1016/j.rse.2005.04.016.

Oigawa, M., T. Matsuda, T. Tsuda, and Noersomadi, 2017: Coordinated observation and numerical study on a diurnal cycle of tropical convection over a complex topography in West Java, Indonesia. *J. Meteor. Soc. Japan*, **95**, 261−281, doi:10.2151/jmsj.2017-015.

Potemra, J. T., and N. Schneider, 2007: Interannual variations of the Indonesian throughflow. *J. Geophys. Res. Oceans*, **112**, C05035, doi:10.1029/2006JC003808.

Qian, J. H., A. W. Robertson, and V. Moron, 2010: Interactions among ENSO, the monsoon, and diurnal cycle in rainfall variability over Java, Indonesia. *J. Atmos. Sci.*, **67**, 35093524, doi:10.1175/2010JAS3348.1.

Rivas, M. B., and A. Stoffelen, 2019: Characterizing ERA-Interim and ERA5 surface wind biases using ASCAT. *Ocean Sci.*, **15**, 831−852, doi:10.5194/os-15-831-2019.

SeaPAC, 2018: QuikSCAT Level 2B Ocean Wind Vectors in 12.5km Slice Composites Version 4.0. PO.DAAC, CA, USA (Available online at: https://doi.org/10.5067/QSX12-L2B40, accessed 2 April 2022).

Short, E., C. L. Vincent, and T. P. Lane, 2019: Diurnal cycle of surface winds in the maritime continent observed through satellite scatterometry. *Mon. Wea. Rev.*, **147**, 2023−2044, doi:10.1175/MWR-D-18-0433.1.

Worku, L. Y., A. Mekonnen, and C. J. Schreck, 2019: Diurnal cycle of rainfall and convection over the Maritime Continent using TRMM and ISCCP. *Int. J. Climatol.*, **39**, 5191−5200, doi:10.1002/joc.6121.

Wood, R., M. Köhler, R. Bennartz, and C. O'Dell, 2009: The diurnal cycle of surface divergence over the global oceans. *Quart. J. Roy. Meteor. Soc.*, **135**, 1484−1493, doi:10.1002/qj.451.

Wu, C.-H., and H.-H. Hsu, 2009: Topographic influence on the MJO in the Maritime Continent. *J. Climate*, **22**, 5433−5448, doi:10.1175/2009JCLI2825.1.

Manuscript received 2 April 2022, accepted 1 June 2022
SOLA: *https://www.jstage.jst.go.jp/browse/sola/*